ADVANCED QUANTUM TECHNOLOGIES
www.advquantumtech.com

Anomalous Loss Reduction Below Two-Level System Saturation in Aluminum Superconducting Resonators

Tamin Tai, Jingnan Cai, and Steven M. Anlage*

Superconducting resonators are widely used in many applications such as qubit readout for quantum computing, and kinetic inductance detectors. These resonators are susceptible to numerous loss and noise mechanisms, especially the dissipation due to two-level systems (TLS) which become the dominant source of loss in the few-photon and low temperature regime. In this study, capacitively-coupled aluminum half-wavelength coplanar waveguide resonators are investigated. Surprisingly, the loss of the resonators is observed to decrease with a lowering temperature at low excitation powers and temperatures below the TLS saturation. This behavior is attributed to the reduction of the TLS resonant response bandwidth with decreasing temperature and power to below the detuning between the TLS and the resonant photon frequency in a discrete ensemble of TLS. When response bandwidths of TLS are smaller than their detunings from the resonance, the resonant response and thus the loss is reduced. At higher excitation powers, the loss follows a logarithmic power dependence, consistent with predictions from the generalized tunneling model (GTM). A model combining the discrete TLS ensemble with the GTM is proposed and matches the temperature and power dependence of the measured internal loss of the resonator with reasonable parameters.

1. Introduction

2D planar high internal quality factor (Q_i) superconducting resonators have been widely fabricated and investigated in recent times for applications such as single photon detectors,[1] kinetic inductance detectors,[2] and quantum buses in quantum computing technology.[3] Tremendous progress has been made in terms of design, fabrication, and measurement techniques, which has led to orders of magnitude increase in coherence time and improved quantum fidelity of the quantum gates.[3-5] In microwave measurements, although all qubits are operated at an excitation frequency well below the superconducting gap energy, microwave photons can be absorbed by quasiparticles, which in turn interact with the phonon bath, creating non-equilibrium distributions of both quasiparticles and phonons.[6-9] This process affects the population of quasiparticles, in addition to pair-breaking process induced by cosmic rays,[10] higher order microwave harmonics, and stray infrared radiation.[11-13] These non-equilibrium quasiparticles are one limiting factor on superconducting resonator Q_i and qubit coherence, which can reduce both the qubit relaxation time (T_1^{Qubit}) and the coherence time (T_2^{Qubit}).[14]

Another comparable loss mechanism due to two-level systems (TLS) is also ubiquitous in 2D superconducting resonators.[15-30] Despite the elusive microscopic origin of the TLS (some recent works suggesting hydrogen impurities in alumina as one candidate for TLS[31,32]), TLS can be simply modeled as electric dipoles that couple to the microwave electric field. In general, TLS are abundant in amorphous solids and can also exist in the local defects of crystalline materials. They are found in three kinds of interfaces in the superconducting resonators: the metal–vacuum interface due to surface oxide or contaminants; the metal–dielectric substrate interface due to residual resist chemicals and buried adsorbates; and the dielectric substrate–vacuum interface with hydroxide dangling bonds, processing residuals, and adsorbates.[33] To address these issues, different kinds of geometry of coplanar waveguide (CPW) structure have been proposed and fabricated, with more care given to the surface treatment to alleviate the TLS losses.[34] For example, a trenched structure in the CPW helps to mitigate the metal–dielectric TLS interaction with the resonator fields.[35,36] These efforts have improved the 2D resonator intrinsic quality factor to more than 1 million in recent realizations of high-Q_i resonators.[35-39] Nevertheless, TLS still exist even in extremely high Q_i 3D superconducting radio frequency cavities used in particle accelerator applications.[40] Recently, other sources of TLS loss have been proposed based on quasiparticles trapped near the surface of a superconductor.[41]

Clearly TLS loss is a universal issue in superconducting resonators. However, at microwave frequencies, this loss was long thought to be constant under low microwave power and low temperature below TLS saturation.[16–18,28,42,43] Measurements in this

T. Tai, J. Cai, S. M. Anlage
Quantum Materials Center, Department of Physics
University of Maryland
College Park, MD 20742-4111, USA
E-mail: jcai@umd.edu

The ORCID identification number(s) for the author(s) of this article can be found under https://doi.org/10.1002/qute.202200145

DOI: 10.1002/qute.202200145

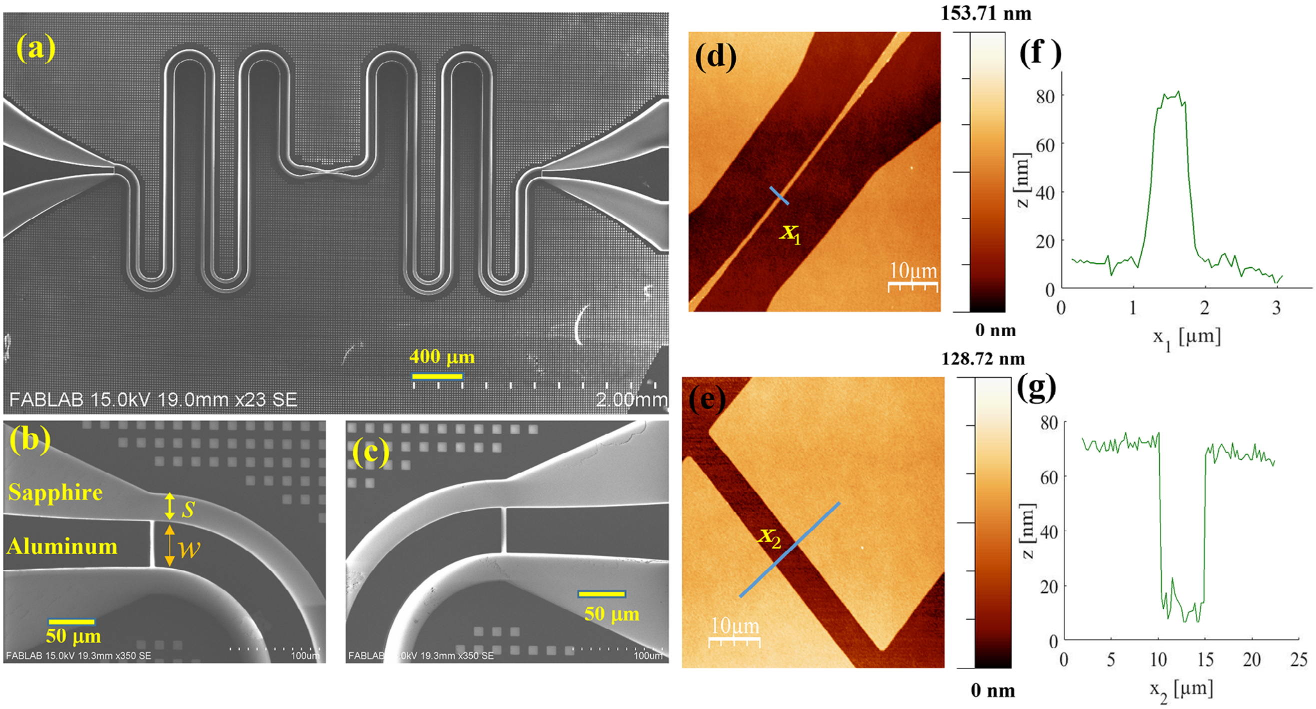

Figure 1. a) An SEM image of the aluminum CPW resonator on a sapphire substrate. b,c) Zoom-in SEM images of the left and right capacitive couplers. d) AFM image highlighting the tapered center conductor with a 1 μm wide center trace near the center of the resonator, and e) AFM topography image highlighting the 5 μm wide capacitive coupler from (b) or (c). Note that the AFM probe scanning direction is 45 degrees with respect to the center-line direction to reduce AFM scanning artifacts. f) Line scan profile of AFM image to show thickness of the center line in (d). g) Line scan profile of the capacitive coupler. Both line scans show an Al film thickness of 70 nm.

regime were limited due to the constraints of noise levels in both electronic equipment and the thermal environment. Therefore, experimental investigation of TLS at low temperatures and microwave excitation are important, and would assist the superconducting quantum information community to understand its effect on operating quantum devices.

We have designed a 2D half wavelength resonator with a tapering geometry that gradually shrinks the signal line width w from 50 μm down to 1 μm at the center where many three-junction flux qubits could be hosted and strongly coupled for the study of the collective behavior of quantum meta-materials. Analogous to cavity quantum electrodynamics, qubits serve as artificial meta-atoms with mutual coupling[44–48] and can be read out through the dispersive frequency shift of the cavity.[49–51] Theoretical publications discussing the physics of qubit arrays coupled to the harmonic cavities predict a number of novel collective behaviors of these meta-atoms.[52–54] In this paper, we report our finding on the TLS loss in the low power and low temperature limit of this particular design of capacitively-coupled half-wavelength resonator, without the qubits. The technique of very low power microwave measurement with low noise to enhance the signal-to-noise ratio (SNR) is critical for measuring this TLS behavior.

2. Experimental Methods

Aluminum (Al) half-wavelength ($\lambda/2$) CPW resonators on sapphire substrates were designed with a center line width $w = 50$ μm and spacing $s = 30$ μm (the distance between center conductor line and ground plane as illustrated in **Figure 1**b to maintain the characteristic impedance near 50 Ω in the meander part. At the center of the resonator a tapering structure narrows the center line width down to $w = 1$ μm and spacing to $s = 12$ μm, which gradually increases the characteristic impedance to 100 Ω at the resonator center. Figure 1a shows a perspective view of the resonator in a diced chip with a designed fundamental frequency around 3.6 GHz. The entire resonator is surrounded by many 10 μm by 10 μm vortex moats. The resonator is symmetric and capacitively coupled through 5 μm gaps (Figure 1b,c) in the center conductor. A topographic image of the narrowed resonator center section is shown in Figure 1d with a critical dimension around $w = 1$ μm in width. Line cuts shown in the AFM images in Figure 1d,e show that the Al film is 70 nm thick.

This CPW resonator was fabricated using standard photolithography procedures. First, a 70 nm thick Al film was deposited on a 3-inch diameter sapphire wafer using thermal evaporation technology with a background pressure of $\approx 3 \times 10^{-7}$ mbar. Then a thin SHIPLEY1813 photo-resist was coated on top of the film and exposed to UV through the designed photomask. The UV exposed wafer was developed and then wet etched by commercial transene aluminum etchant. The remaining photoresist was stripped off by acetone and the entire wafer was cleaned by methanol and isopropanol. Finally, the wafer was coated in a protective photo-resist and then diced into many chips. After dicing, the protective photo-resist was removed and the chip was mounted on a printed circuit board bolted inside a copper box. Several lumps of indium were pressed between the on-chip

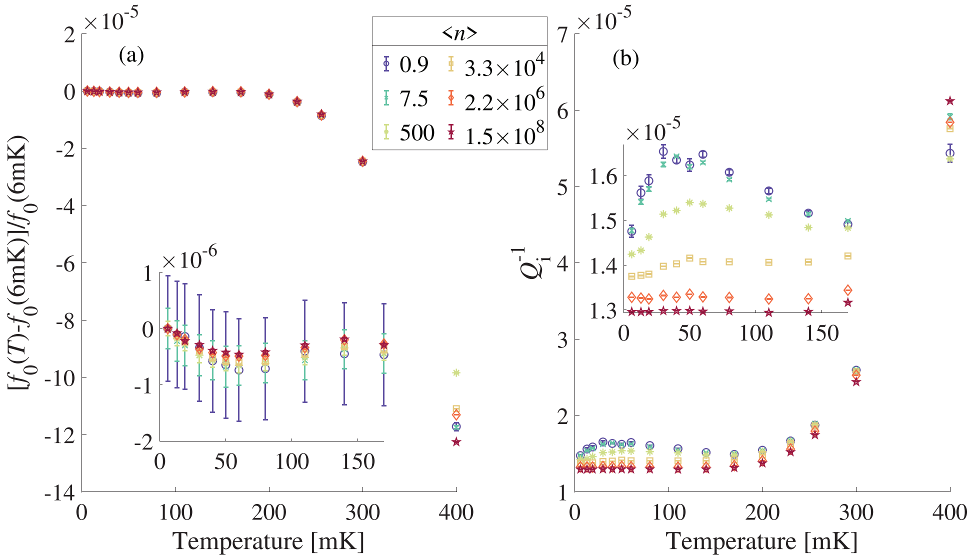

Figure 2. a) Temperature dependent first harmonic resonant frequency shift $\Delta f/f_0(6\text{ mK})$, with $\Delta f = f_0 - f_0(6\text{ mK})$ of the $\lambda/2$ aluminum co-planar waveguide resonator on sapphire substrate measured at different excitation powers (average photon numbers). Here f_0 (6 mK) is the resonance frequency measured at the base temperature for each excitation power . b) Temperature dependent loss (inverse of intrinsic quality factor, Q_i^{-1}) at its first harmonic frequency of an aluminum co-planar waveguide resonator on sapphire substrate measured at different circulating photon numbers $\langle n\rangle$. Some of the error bars are smaller than the data point such as those for the high power and temperature measurements.

ground planes and the copper box ground to achieve a continuous ground contact, which mitigates parasitic resonant microwave modes due to uneven electrical grounding. The indium lumps also secured the chip in the center of the printed circuit board. The on-chip transmission line is wire-bonded to the center conductor of the transmission line on the printed circuit board by gold wires. Finally, the copper box is capped by a copper lid to eliminate stray light illumination.

The device was placed in a closed Cryoperm cylinder in a Blue-Fors (BF-XLD 400) croygen-free dilution refrigerator (base temperature 10 mK) to minimize any stray DC magnetic field, and the shield was thermally anchored to the mixing chamber plate. The microwave excitation was attenuated by a series of attenuators in the input line at different cooling stages in the dilution fridge before going into the resonator to reduce the noise. The transmitted signal was amplified twice through a cryogenic amplifier and a room temperature amplifier before being measured by a Keysight N5242A vector network analyzer (VNA). The low power measurements were performed using the smallest intermediate frequency bandwidth (1 Hz) of the VNA, with a 400 kHz span across the resonance, following five averages to reduce the random noise. A thru calibration of the setup was performed in a separate cool down to determine the overall loss/gain in the transmission lines leading to the resonator. Further details of the experimental setup for the high SNR measurement at very low microwave power can be found in Section S1, Supporting Information.

3. Experimental Data

The measured transmitted signal ($S_{21}(f)$) has a fundamental ($\lambda/2$) resonance peak around $f = 3.644$ GHz at the fridge base temperature when sweeping the frequency, f. The complex $S_{21}(f)$ signal is fitted to an equivalent circuit model of a two-port resonator capacitively coupled to external microwave excitation.[9,55]

$$S_{21}(f) = |S_{21,\mathrm{in}}||S_{21,\mathrm{out}}|\left(\frac{Q_L/Q_c}{1+2iQ_L(\frac{f}{f_0}-1)}e^{i\phi}\right) + C_0 \tag{1}$$

where $|S_{21,\mathrm{in}}|$ and $|S_{21,\mathrm{out}}|$ are the net loss or gain in the transmission of the input and output line, respectively. Q_L is the loaded quality factor. Q_c is the coupling quality factor representing the dissipation to the external circuit, $i=\sqrt{-1}$, f_0 is the resonance frequency of the half-wavelength ($\lambda/2$) CPW resonator, ϕ is the phase and C_0 is an offset in the complex S_{21} plane due to background contributions.[55] The internal quality factor, Q_i, inversely proportional to the internal loss, $\delta = Q_i^{-1}$, is extracted from the identity $1/Q_L \equiv 1/Q_i + 1/Q_c$. The absorbed power P_{ab} of the resonator is characterized by the average number of circulating microwave photons in the cavity on resonance, which can be estimated using the approximation[9,56] $\langle n\rangle = \frac{2Q_L^2 P_{\mathrm{in}}}{Q_c \hbar\omega_0^2}$ for a two-port device, where $\hbar$ is the reduced Planck constant, and $\omega_0 = 2\pi f_0$ is the angular frequency of the resonance.

Figure 2a illustrates the temperature dependence of the fractional resonant frequency shift from the resonance frequency at lowest temperature, $(f_0(T) - f_0(6\text{ mK}))/f_0(6\text{ mK})$, for different circulating microwave photon numbers inside the CPW resonator, where 6 mK is the measured fridge base temperature. The resonance frequencies start at their maxima at the fridge base temperature and then show local minima ≈60 mK. This phenomenon seems to be independent of the average circulating photon number and can be explained by the standard tunneling model (STM) of TLS.[43] Upon further increasing the temperature above 150 mK, the resonance frequencies quickly decrease due to the thermal quasiparticles, which increases the real and imaginary parts of the surface impedance of the superconducting resonator. The inset focuses on the low temperature regime and shows a very small power dependence that is qualitatively similar to the strong field correction to the frequency shift in the STM proposed by Gao, which predicts smaller frequency shifts for higher power.[57]

The temperature dependence of the measured internal loss is shown in Figure 2b. For high power measurements ($\langle n \rangle > 10^6$), the loss is constant at low temperatures (below 150 mK) which is expected for the typical non-interacting TLS. At higher temperatures, the loss increases due to thermal quasiparticles. For low power measurements ($\langle n \rangle < 10^6$), starting from the minimum temperature, the loss has an unusual increase at low temperatures, from the base temperature to a peak at 40 mK. The loss then drops with increasing temperature following the equilibrium value of the population difference in TLS.[20,58] Similar to the high power measurements, the loss rises again above 150 mK due to thermal quasiparticles. The observed loss decrease with decreasing temperature from 40 to 10 mK has not been explicitly acknowledged and discussed in prior work of microwave superconducting resonators until recently.[59] Indications of an upturn in $Q_i(T)$ has otherwise been attributed to poor SNR and therefore treated as not statistically significant.[58,60]

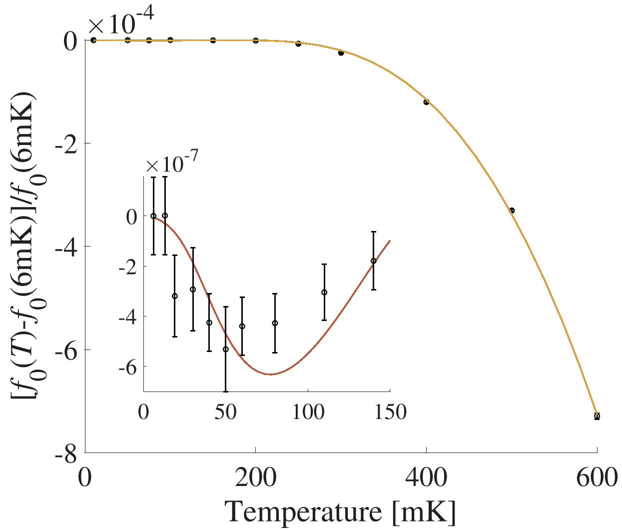

Figure 3. Temperature dependent fundamental ($\lambda/2$) mode resonant frequency $f_0(T)$ of the Al CPW resonator on sapphire substrates at an external microwave excitation creating around one circulating photon. The inset highlights the low temperature regime where the frequency shift is dominated by the TLS mechanism. The dots are experimental data and solid line is the model fit to Equation (2).

4. Modeling

4.1. Frequency Shifts

The power and temperature dependent frequency shifts are explained by the TLS and the dynamics of quasiparticles. These two mechanisms could overlap and become difficult to distinguish in the operation of many superconducting devices, including resonators and qubits.[14] A simple model that combines both quasiparticles and TLS contribution in one equation describes the resonance frequency Δf data in Figure 2[25,34,61]

$$\frac{f_0(T)-f_0(0)}{f_0(0)} = \frac{\delta_0}{\pi}\left(\mathrm{Re}\left[\Psi\left(\frac{1}{2}+\frac{\hbar\omega}{2\pi i k_B T}\right)\right]-\log\left(\frac{\hbar\omega}{2\pi k_B T}\right)\right) - \frac{\alpha}{2}\left(\frac{n_{qp}}{2N_0\Delta_{S0}}\left[1+\sqrt{\frac{2\Delta_{S0}}{\pi k_B T}}\exp(\zeta)I_0(\zeta)\right]\right) \tag{2}$$

where $\zeta = \frac{hf_0}{2k_B T}$, f_0 is the resonance frequency as a function of the temperature, δ_0 is the zero temperature and zero power loss tangent from the TLS, $\Psi(\cdot)$ is the digamma function, $\alpha = L_{\mathrm{kinetic}}/L_{\mathrm{total}}$ is the kinetic inductance fraction of the CPW resonator, N_0 is the single spin density of states, Δ_{S0} is the aluminum superconducting gap at zero temperature, and $I_0(\cdot)$ is the 0th order modified Bessel function of the first kind. The first term in Equation (2) represents the frequency shift caused by the TLS mechanism[20,23] and the second term is the frequency shift due to quasiparticles using the Bardeen–Cooper–Schrieffer (BCS) model for $k_B T$, $hf_0 \ll \Delta_{S0}$, and written explicitly in terms of quasiparticle number density n_{qp},[61] including both thermal and non-equilibrium quasiparticles. However, the model with only thermal quasiparticle $n_{th} = 2N_0\sqrt{2\pi k_B T \Delta_{S0}}\exp(-\frac{\Delta_{S0}}{k_B T})$ (valid for $T \ll T_c$) seems to match the measurement sufficiently well, where $N_0 = 10^{47}\ \mathrm{J^{-1}\,m^{-3}} \approx 1.74\times10^4\,\mathrm{\mu eV^{-1}\mu m^{-3}}$ is the single spin electronic density of states at the Fermi level.[7,13]

The fit to the frequency shift data is shown in **Figure 3**, and the extracted fitting parameters indicate that the aluminum superconducting gap at zero temperature is $\Delta_{S0} \approx 170$ µeV, a value close to the BCS gap approximation which is $1.76k_B T_c$ with transition temperature $T_c = 1.12$ K. The values of the other fitting parameters are $\alpha \approx 0.014$, and $\delta_0 = 9.6\times10^{-6}$. The values of α and δ_0 are consistent with other results on a variety of similar superconducting resonators.[23,27,34,62]

4.2. Internal Loss

Since the temperature dependent internal loss is dominated by the well-known thermal quasiparticles above 150 mK, this analysis focuses only on the low temperature data. The power dependence of the loss $Q_i^{-1}(T)$ is shown in **Figure 4** at different temperatures below the onset of thermal quasiparticle effects. Clearly, the loss shows a gradual power dependence above the low-power saturation, similar to previous experimental observations,[27,37,63,64] and is not consistent with STM shown as the dashed curves.

To account for the slower power dependence, many improvements on the STM have been proposed, such as introducing more than one species of TLS in the dielectrics,[65–69] and accounting for the nonuniform field distribution in the resonator.[24] In addition, there is another approach that generalizes the STM to include a random telegraph noise on the TLS energy level due to strong interactions between a few TLS,[70–72] resulting in the generalized tunneling model (GTM) that can produce the logarithmic power dependence shown as the black dotted line in Figure 4.

However, none of the existing models predicts a strong temperature dependence of loss below the TLS saturation. To inter-

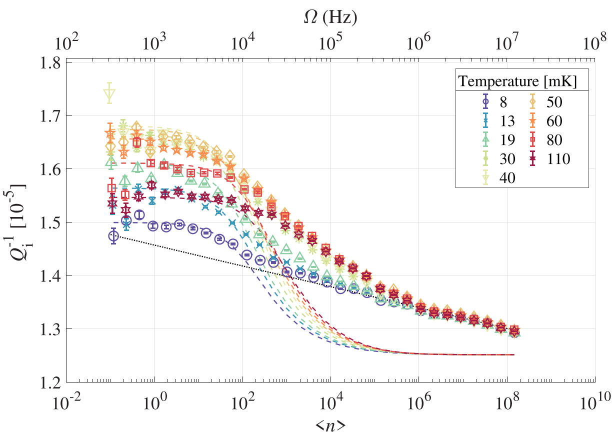

Figure 4. Internal loss Q_i^{-1} as a function of power (measured by photon number $\langle n\rangle$ on lower axis, and Rabi frequency Ω on upper axis) at different temperatures for an aluminum resonator on a sapphire substrate. The scatter plots are experimental data points, and the dashed lines are the fitting curves from the STM given in Equation (8). There is a large deviation from STM power dependence at high power above TLS saturation power. The power dependence is more gradual than the STM prediction, and the loss has very weak temperature dependence, which resemble the logarithmic power dependence predicted by GTM. The black dotted line is the power dependence at high excitation power from GTM. A constant background loss is assumed for all the fits.

pret this unusual loss reduction in our aluminum resonators at low power and low temperature, we go beyond the assumption of a uniform distribution of TLS and invoke the discrete TLS contribution to the loss at low temperatures. A simple modification that sums over the discrete and detuned TLS responses near the resonance as in Equation (14) is proposed. When combined with GTM, this model reproduces the full power and temperature dependence of the loss data: the gradual power dependence at high power as well as the observed anomalous temperature dependence of loss for $\langle n\rangle < 10^2$ and $T < 50$ mK. It should be emphasized that the discrete TLS assumption is independent of GTM. Attempts to apply the discrete and detuned TLS formalism to the modified versions of STM are summarized in Section S4, Supporting Information. To lay the foundations of the proposed model, the following sections introduce key concepts of STM and GTM and derive several expressions used in the final model.

4.2.1. Conventional Model for TLS Loss

The TLS formalism is based on a simple model for a single TLS that can be described by the Hamiltonian, $H_{\mathrm{TLS}} = \frac{1}{2}\begin{pmatrix} -\Delta & \Delta_0 \\ \Delta_0 & \Delta \end{pmatrix}$ where Δ is the asymmetry of the double well potential and Δ_0 is the tunneling barrier energy between the potential wells.[20] A typical resonator hosts an ensemble of TLS with different values of Δ and Δ_0 with their (assumed continuous) distribution function given as $P(\Delta, \Delta_0) = P_0/\Delta_0$, where $P_0 \approx 10^{44}\,\mathrm{J^{-1}m^{-3}}$ is the density of states for TLS. The distribution function is uniform in Δ in the conventional TLS model, but could take on a very weak dependence $\propto \Delta^{\mu}$ with $\mu \approx 0.3$ for a system of very strongly interacting TLS,[72–74] such as the case assumed in GTM. For simplicity and generality, the following model uses the conventional distribution function, which is constant in Δ. The fit with nonzero μ can be found in the Section S4, Supporting Information.

The dynamics of a single TLS can be described by the linearized Bloch equations of the pseudospin $\vec{S}(t)$ (see Section S2, Supporting Information for details) that is characterized by the following four rates: Rabi frequency $\Omega \propto |\vec{E}|$, the frequency of the driving field ω, the splitting between the two eigenenergies of TLS $\varepsilon = \sqrt{\Delta^2 + \Delta_0^2}$, and the longitudinal and transverse relaxation rates of the TLS $\Gamma_{1,2}$ which are defined as

$$\Gamma_1 = \left(\frac{\Delta_0}{\varepsilon}\right)^2 \left[\frac{\gamma_L^2}{v_L^5} + \frac{2\gamma_T^2}{v_T^5}\right] \frac{\varepsilon^3}{2\pi\rho\hbar^4} \coth\left(\frac{\varepsilon}{2k_B T}\right)$$

$$= \left(\frac{\Delta_0}{\varepsilon}\right)^2 \Gamma_1^{\max} \quad [18, 42, 43, 57] \tag{3}$$

$$\Gamma_2 = \Gamma_2^{\mathrm{ph}} + \Gamma_{\mathrm{ds}}$$

$$\text{where} \quad \Gamma_2^{\mathrm{ph}} = \Gamma_1/2 \quad \text{and}$$

$$\Gamma_{\mathrm{ds}} \approx 10^{-3}(k_B T/\varepsilon_{\max})^{\mu} k_B T/\hbar \quad [72, 75] \tag{4}$$

Equation (3) describes the longitudinal relaxation rate dominated by the phonon process where γ_L and γ_T are the longitudinal and transverse deformation potentials, respectively, v_L and v_T are the longitudinal and transverse sound velocities, ρ is the mass density, and $\Gamma_1^{\max}$ is the maximum Γ_1 for the TLS with energy splitting ε, when $\Delta_0 = \varepsilon$. Equation (4) defines the transverse relaxation rate where Γ_{ds} is the dephasing rate of the resonant TLS energy level ε, caused by its interactions with thermally activated TLS whose $\varepsilon \lesssim k_B T$, and is valid for low temperature measurement ($T < 1$ K).[75] We note that $\mu = 0$ for the conventional TLS model used here, and $\Gamma_{\mathrm{ds}} \approx 10^6$ Hz dominates over $\Gamma_1 \approx 10^3$ Hz in the typical cryogenic measurement of amorphous dielectrics.[72] Therefore, Γ_2 is often approximated as Γ_{ds} and is proportional to T.

In STM, the resonant dielectric response of a single TLS is expressed as[15,17,71]

$$\chi_{\mathrm{res}} = \frac{m(\omega - \varepsilon/\hbar - i\Gamma_2)}{(\omega - \varepsilon/\hbar)^2 + \Gamma_2^2(1 + \Omega^2\Gamma_1^{-1}\Gamma_2^{-1})} \tag{5}$$

where $m = \tanh(\varepsilon/(2k_B T))/2$ is the equilibrium value of $\langle S_z^0\rangle$. The single TLS loss corresponds to the imaginary part of the response function in Equation (5) which is in the form of a Lorentzian in $\varepsilon/\hbar$ centered at ω with a width

$$w = \Gamma_2\sqrt{1 + \kappa} \tag{6}$$

where $\kappa = \Omega^2\Gamma_1^{-1}\Gamma_2^{-1}$. For a typical TLS with $\varepsilon/h \approx 5$ GHz and at reasonably low temperatures and powers, the width of its response $w \approx \Gamma_2 \approx 1$ MHz $\ll \omega$. Due to this sharp Lorentzian response function, the total loss is dominated by the resonant TLS whose energies $\varepsilon \approx \hbar\omega$.

The total dielectric loss is simply the integral of the single TLS contribution Equation (5) over the distribution of the TLS.[17,20,57]

$$\delta_{\mathrm{TLS}} = \frac{1}{\epsilon_{\mathrm{r}}\epsilon_0} \int\int\int P(\varepsilon, \Delta_0)\left(\frac{\Delta_0 d_0}{\varepsilon}\right)^2 \frac{\cos^2\theta}{\hbar} \times \frac{m\Gamma_2}{\Gamma_2^2(1+\kappa) + (\varepsilon/\hbar - \omega)^2} \mathrm{d}\varepsilon \mathrm{d}\Delta_0 \mathrm{d}\theta \tag{7}$$

where $\epsilon_{\mathrm{r}}\epsilon_0$ is the permittivity of the host dielectric material, $P(\varepsilon, \Delta_0)$ is the distribution function of coherent TLS, obtained from $P(\Delta, \Delta_0)$ with a change of variable from Δ to ε, d_0 is the maximum transition electric dipole moment of the TLS with energy splitting ε, $\vec{E}$ is the applied microwave electric field on the TLS dipole, and θ is the angle between the applied electric field and the TLS dipole moment.

Evaluating this integral leads to the famous STM prediction of TLS loss[43]

$$\delta_{\mathrm{TLS}} = \frac{\pi P_0 d_0^2}{3\epsilon_{\mathrm{r}}\epsilon_0} \frac{\tanh\frac{\hbar\omega}{2k_{\mathrm{B}}T}}{\sqrt{1+(\Omega/\Omega^{\mathrm{c}})^2}} \tag{8}$$

where $\Omega^{\mathrm{c}} \propto \sqrt{\Gamma_1^{\max}\Gamma_2}$ is the critical Rabi frequency that characterizes the saturation of TLS. The loss is expected to have an inverse square root dependence on power after the TLS saturation, $\delta_{\mathrm{TLS}} \sim \Omega^{-1} \propto P_{\mathrm{ab}}^{-0.5}$ for $\Omega \gg \Omega^{\mathrm{c}}$, which is much faster than observed in the data in Figure 4. In fact, if one fits the data with a general power law[27] where the square root in the denominator of Equation (8) is replaced by a fitting parameter, the resulting exponent is around −0.15, indeed a slower power dependence than predicted in STM.

4.2.2. Effect of Fluctuators on TLS Loss

The dephasing rate Γ_{ds} introduced in Equation (4) describes the spectral diffusion resulting from an average of weak interactions among TLS,[20,72] which cannot incorporate stochastic and discrete strong interactions following a Poisson process, such as those from fluctuators.[70–72,76–78] Fluctuators can be modeled as incoherent TLS whose $\Gamma_2^{\mathrm{ph}} \geq \varepsilon$, as opposed to the coherent TLS introduced above in STM.[72] If strongly coupled with the coherent resonant TLS, the fluctuators can move the latter in and out of resonance with a jump rate γ and effectively create a random telegraphic noise on the energy level $\varepsilon \to \varepsilon + \xi(t)$. The fluctuators can be modeled as following a thermally activated tunneling process with rate $\gamma = \gamma_0 \exp(\frac{-E_{\mathrm{a}}}{k_{\mathrm{B}}T})$, where E_{a} is the activation energy. For a uniform distribution of $E_a \in [E_{\mathrm{a,min}},\ E_{\mathrm{a,max}}]$, the distribution of the fluctuator rates is thus $P(\gamma) \sim 1/\gamma$ in an exponentially wide range $[\gamma_{\min}, \gamma_{\max}]$, with $\gamma_{\min} = \gamma|_{E_{\mathrm{a}}=E_{\mathrm{a,max}}} \approx$ constant in T and $\gamma_{\max} = \gamma|_{E_{\mathrm{a}}=E_{\mathrm{a,min}}} \propto \exp(\frac{-E_{\mathrm{a,min}}}{k_{\mathrm{B}}T})$.[71,72] The random telegraphic noise with a slow jump rate γ happens infrequently during the measurement time, and thus cannot be averaged over to contribute to the spectral diffusion as in Equation (4). The exact solution to the Bloch equation will depend on the relationship between $\gamma, \Omega, \Gamma_1^{\max}$, and Γ_2. $\Gamma_1^{\max}$ is abbreviated to Γ_1 for clarity in the following discussion, which mainly focuses on the interaction between fluctuators and one resonant TLS. Thus, the distribution of values of Γ_1 for an ensemble of TLS is not invoked until the last step of integration to calculate the loss, and is not relevant to the fluctuators-induced effect.

When the jump rate γ is slow compared to the dynamics of the resonant TLS characterized by the rates $\Omega, \Gamma_1, \Gamma_2$, the stationary solution similar in form to Equation (5) can still be used with the substitution $\varepsilon \to \varepsilon + \xi$. After averaging over the distribution of the fluctuator jumps ξ, the response of a single TLS weakly coupled to low-γ fluctuators is obtained (see Section S3, Supporting Information)

$$\chi_{\mathrm{res}} = m\frac{\omega - \varepsilon/\hbar - i(\Gamma_2 + \Gamma_{\mathrm{f}}/\sqrt{1+\kappa})}{(\Gamma_2\sqrt{1+\kappa} + \Gamma_{\mathrm{f}})^2 + (\omega - \varepsilon/\hbar)^2} \tag{9}$$

which has the same form as Equation (5) but with the width of the Lorentzian widened by $\Gamma_{\mathrm{f}} \propto T \lesssim \Gamma_2$ due to the weakly-coupled low-γ fluctuators.[72] For a continuous distribution of TLS such as $P(\varepsilon, \Delta_0)$, the total internal loss is calculated by integrating Equation (9) over the distribution function $P(\varepsilon, \Delta_0)$ and $P(\gamma)$ in the range $\gamma \in [\gamma_{\min}, \Gamma_1]$.

$$\delta_{\mathrm{TLS}} = \frac{1}{\epsilon_{\mathrm{r}}\epsilon_0}\int\int\int\int P(\varepsilon, \Delta_0)P(\gamma)\left(\frac{\Delta_0 d_0}{\varepsilon}\right)^2 \frac{\cos^2\theta}{\hbar}\frac{m}{\sqrt{1+\kappa}} \times \frac{(\Gamma_2\sqrt{1+\kappa} + \Gamma_{\mathrm{f}})}{(\Gamma_2\sqrt{1+\kappa} + \Gamma_{\mathrm{f}})^2 + (\varepsilon/\hbar - \omega)^2}\mathrm{d}\varepsilon\mathrm{d}\Delta_0\mathrm{d}\theta\mathrm{d}\gamma \tag{10}$$

Clearly, the last fraction in the integral is a Lorentzian which evaluates to a constant after integration over ε, resulting in the same prediction for internal loss as the STM.[72]

On the other hand, when the dynamics of the resonant TLS is dominated by a fast jump rate, $\gamma \gtrsim \Omega, \Gamma_1, \Gamma_2$, a probabilistic description of the resonant TLS must be adopted. Instead of directly solving the linearized Bloch equations Equations (S2) and (S3), Supporting Information, the master equation or the evolution equation of the probability distribution $\rho(\vec{S})$ of the Bloch vector $\vec{S} = (\langle S_x^1\rangle, \langle S_y^1\rangle, \langle S_z^0\rangle)$ is introduced[71]

$$\frac{\partial\rho}{\partial t} + \frac{\mathrm{d}}{\mathrm{d}\vec{S}}(\frac{\mathrm{d}\vec{S}}{\mathrm{d}t}\rho) = \gamma[\delta(S_z^0 - m)\delta(S_x^1)\delta(S_y^1) - \rho] \tag{11}$$

where $\mathrm{d}\vec{S}/\mathrm{d}t$ is given in Equation (S2) and (S3) with a time independent ε where the random jumps $\xi(t)$ are dropped since the fast jumps are averaged out over a long time. (See Section S3, Supporting Information). The TLS loss is then extracted by solving for the average y component of $\vec{S}$, $\overline{\langle S_y^1\rangle} = \int \rho\langle S_y^1\rangle \mathrm{d}\vec{S}$, and integrating the solution over the probability distribution of fast fluctuator jump rates $P(\gamma) \propto 1/\gamma$ where $\gamma \in [\max(\Omega, \Gamma_2), \gamma_{\max}]$, and the distribution of resonant TLS energies $P(\varepsilon, \Delta_0)$. The loss has a logarithmic dependence on power

$$\delta = m\delta_0 \mathrm{arcsinh}\left(\frac{\gamma}{\Omega}\right)\Bigg|_{\max(\Omega,\Gamma_2)}^{\gamma_{\max}} \xrightarrow{\gamma_{max}\gg\Omega\gg\Gamma_1,\Gamma_2} m\delta_0\ln(\frac{\gamma_{\max}}{\Omega}) \tag{12}$$

This expression explains the high power limit of the data in Figure 4 where the losses from different temperatures converge to a linear trend in the linear-log plot. This high γ fluctuator loss will saturate to a constant value $\approx m\ln(\gamma_{\max}/\Gamma_2)$ once $\Omega \lesssim \Gamma_2$ (See Section S3, Supporting Information). Thus, it will not affect the low power behavior of the TLS loss.

More complicated is the case of intermediate jump rates where $\gamma \approx \Omega, \Gamma_1, \Gamma_2$. A similar master equation as in Equation (11) needs to be solved with $\varepsilon \to \varepsilon + \xi_k$ for each different fluctuator state k. The jumps are no longer ignored since their rates are close to the other dynamics $(\Omega, \Gamma_2, \Gamma_1)$ in the system. After obtaining the average solution $\overline{\langle S_y^1\rangle}$ for the TLS with energy levels ε_k, the same recipe for the loss calculation can be applied, namely, integrating the average solution over $P(\gamma)$ and then integrating over the distribution of the coherent TLS $P(\varepsilon, \Delta_0)$. The loss is then (See S3, Supporting Information)

$$\delta = \delta_0 \int \frac{m\Gamma_2}{\Gamma_2^2 + (\varepsilon - \omega)^2}\left(\frac{1}{1+\kappa(\varepsilon)}\ln\frac{\gamma_\mathrm{h}}{\gamma_\mathrm{l}} + \frac{\kappa(\varepsilon)(1-n)}{(1+\kappa(\varepsilon))(1+n\kappa(\varepsilon))}\ln\frac{1+\kappa(\varepsilon)+\gamma_\mathrm{h}/\Gamma_1(1+n\kappa(\varepsilon))}{1+\kappa(\varepsilon)+\gamma_\mathrm{l}/\Gamma_1(1+n\kappa(\varepsilon))}\right)\mathrm{d}\varepsilon \tag{13}$$

where $\kappa(\varepsilon) = \Xi/\Gamma_1 = \Omega^2\Gamma_2/[(\varepsilon/\hbar - \omega)^2 + \Gamma_2^2]/\Gamma_1$, and n is the probability that a given TLS is resonant, and is typically small for a system of many (≈ 10) fluctuators (see Supporting Information[71]), and thus ignored in the final model. $\gamma_{\mathrm{h,l}}$ are the upper and lower bounds of the jump rates and are defined such that $\gamma_\mathrm{h} \gtrsim \Xi + \Gamma_1, \sqrt{\Gamma_2^2 + (\varepsilon/\hbar - \omega)} \gtrsim \gamma_\mathrm{l}$. These limits translate to a range for power Ω where the power dependence of the loss is dominated by this model: $\Gamma_2 \gtrsim \Omega \gtrsim \sqrt{\Gamma_1\Gamma_2}$. Within this range, the loss from intermediate γ fluctuators is approximately $\delta_0 \ln[(\Omega^2 + \Gamma_2^2)/(2\Omega^2)]$, a faster logarithmic power dependence than Equation (12). At higher powers, the loss becomes constant $\approx\ m\ln(2)$. At lower power, the loss saturates to another constant $m\ln(\Gamma_2/\Gamma_1)$.

In summary, the three different fluctuation rates correspond to three different power ranges for the power dependence of the loss. In the high power limit $\Omega \gtrsim \Gamma_2$, the effect of fluctuators that induce large γ dominates and leads to a logarithmic power dependence; in the intermediate power regime $\Gamma_2 \gtrsim \Omega \gtrsim \sqrt{\Gamma_1\Gamma_2}$, the fluctuators with intermediate γ give rise to a faster logarithmic power dependence, but meanwhile the saturation of TLS just as in STM has a comparable or even stronger power dependence and overlap in the same power regime; and finally in the low power limit $\Omega < \sqrt{\Gamma_1\Gamma_2}$, the typical TLS saturation in STM is recovered as the contributions from all three different types of fluctuators become constant in power. The above description qualitatively matches our experimental observation in Figure 4.

4.2.3. Fit to the Internal Loss Measurements

Although the power dependence of our data as in Figure 4 agrees with the effect of fluctuators in the GTM, the original model does not reproduce the observed temperature dependence. The GTM predicts the same temperature dependence of the TLS loss in the low power limit as in STM[72] shown as the orange dashed curve in **Figure 5**b, which clearly deviates from the extracted low power loss of TLS. To reconcile this difference, we propose a simple modification to the TLS model to account for the discrete coherent TLS near the resonance. Consider the discrete form of the integral in the TLS loss for low γ fluctuators, Equation (10)

$$\delta_{\mathrm{TLS}} = \frac{P_0 d_0^2 \Delta\varepsilon}{3\hbar\varepsilon_\mathrm{r}\varepsilon_0}\ln\left(\frac{\Gamma_1}{\gamma_{\min}}\right)\sum_n \tanh\left(\frac{\varepsilon_n}{2k_\mathrm{B}T}\right) \times \frac{\Gamma_2 + \Gamma_\mathrm{f}/\sqrt{1+\kappa}}{(\Gamma_2\sqrt{1+\kappa} + \Gamma_\mathrm{f})^2 + (\varepsilon_n/\hbar - \omega)^2} \tag{14}$$

where the index n denotes the coherent TLS near the resonance and $\Delta\varepsilon$ is the average energy spacing in the TLS spectrum. We believe that Equation (14) is justified since the number of coherent TLS inside the resonator bandwidth is ≈ 1 for a TLS volume around $100\,\mu\mathrm{m}^3$,[79] and many previous works have observed individual TLS in microwave resonators.[80–83] For the TLS exactly on resonance, $\varepsilon = \hbar\omega$, its loss $\delta_{\mathrm{TLS}}\ \approx\ \Gamma_2^{-1} \propto T^{-1}$ at low power, and is the classic result for the single TLS model in STM.[84] However, this stands in clear contrast to the observed reduction in loss at low temperature in Figures 2b and 5.

It is thus required that the TLS is not always on resonance ($\nu = \varepsilon_0/\hbar - \omega \neq 0$ where ε_0 stands for the energy level of the coherent TLS closest to resonance), a reasonable assumption given the sparse TLS distribution in the frequency spectrum for a small volume of TLS-inhabiting dielectrics. Mathematically, the width of the Lorentzian in the summation $w = \Gamma_2\sqrt{1+\kappa} + \Gamma_\mathrm{f}$ dictates the transition from the low temperature reduced loss to the high temperature equilibrium result. For small w, a discrete sum will deviate from the integral since the Lorentzian is under-sampled. While for a Lorentzian with large w, a discrete sum with the same sampling rate will approximate the integral better. Specifically, at low powers ($\kappa \ll 1$), $w = \Gamma_2 + \Gamma_\mathrm{f}$ increases with the temperature and $w = \Gamma_2 + \Gamma_\mathrm{f} \approx\ \nu$ marks the transition temperature between the two regimes. For low temperatures ($w \ll \nu$), the Lorentzian term becomes roughly proportional to $w = \Gamma_2 + \Gamma_\mathrm{f}$ which gives the almost linear temperature dependence of loss. For higher power, w increases with κ, which pushes the transition temperature lower and suppresses the low temperature reduction in loss. And eventually at high powers ($\kappa \gg 1$) such that $w > \nu$ for all temperatures, the equilibrium temperature dependence $m = (1/2)\tanh(\hbar\omega/(2k_\mathrm{B}T))$ in STM is recovered in the entire temperature range. The same discrete summation can be applied to Equation (13) for intermediate γ fluctuators. On the other hand, Equation (12) for high γ fluctuators is only modified with the substitution $\Gamma_2 \to \sqrt{\Gamma_2^2 + \nu^2}$ due to the sparse TLS assumption (See Section S3, Supporting Information). The final model that combines all three contributions is able to reproduce the full temperature ($T = 8$–110 mK) and power ($\langle n\rangle = 10^{-1}$–$10^8$) dependence of the loss shown as the solid curves in Figure 5a.

The fit shows reasonable agreement with the data, with root mean squared error RMSE = 0.0124. There are in total ten fitting parameters, fewer degrees of freedom compared to fitting the data from different temperatures individually. The different contributions to the loss below TLS saturation power are plotted in Figure 5b illustrating that the discrete TLS coupled to low

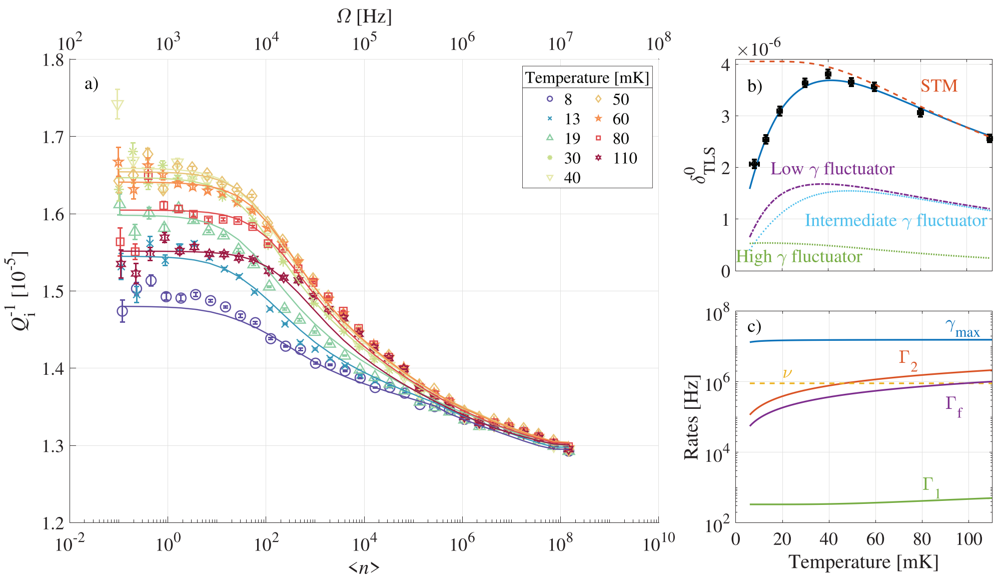

Figure 5. a) The least squares fit of the discrete GTM, together with a constant background loss, to the full power and temperature dependence of the measured internal loss below 150 mK b) Plot of $\delta^0_{TLS}(T)$ extracted from the average of the low power loss below TLS saturation in Figure 4. The orange dashed curve is the temperature dependence of STM loss below saturation power $\propto \tanh(\epsilon/(2k_B T))$. The purple dash-dotted (light blue densely dotted) curve is from the discrete summation of individual TLS contributions for low (intermediate)-γ fluctuators at zero applied power. The green dotted curve is the temperature dependent low power limit of the TLS loss induced by high-γ fluctuators. The blue solid curve is the sum of contributions from the low, intermediate, and high-γ fluctuators. c) Comparison of the temperature dependent rates determined from the least squares fit.

and intermediate γ-fluctuators are responsible for the loss reduction. The different rates in the model determined from the fit are summarized in Figure 5c. The numerical values for $\Gamma_{1,2}$ and $\gamma_{max,min}$ are typical for TLS in amorphous materials.[72] The rates also satisfy the following assumptions in the model: $\Gamma_2 \gtrsim \Gamma_f$, and $\gamma_{max} \gg \Gamma_2$. In addition, the low temperature loss reduction occurs around 40 mK as expected, when $\Gamma_2 + \Gamma_f < \nu$, the width of the response is smaller than the detuning between TLS and the resonance. The other quantities extracted from the fit are listed below: the volume of TLS-inhabiting dielectrics, 10 µm^3, the intrinsic TLS loss, $\delta_0^{TLS} = 3.85 \times 10^{-6}$, the other loss, $\delta_{other} = 1.29 \times 10^{-5}$, and the minimum fluctuator rate $\gamma_{min} = 4.5 \times 10^{-2}$ Hz.

5. Discussion

The discrete and detuned TLS formalism will not affect the high γ-fluctuator contribution to internal loss, since the width of Lorentzian in the calculation of loss of high γ fluctuators w is widened by γ such that $w \approx \gamma > \Delta\epsilon/\hbar$ (See Section S3, Supporting Information), which is indicated by the almost flat region in the green dotted curve at low temperature in Figure 5b. However, the loss from intermediate γ fluctuators could be subject to the low coherent TLS density but to a lesser degree than that from the low γ fluctuators, since although the bandwidth of their response $\approx \Gamma_2$ is the same (See Section S3, Supporting Information), there are many intermediate-γ-fluctuator-induced sublevels for one TLS in one Rabi cycle which effectively increases the density of available TLS energy levels. In order to avoid over fitting, this effect was not included in the model where the same density of states for TLS are assumed for those coupled to intermediate γ fluctuators and the low γ fluctuators. Thus, the same $\Delta\epsilon$ value is shared for the two different contributions. This simplification could lead to an underestimation of the loss in the intermediate power region, as illustrated by the deviation between the fit and data from $\langle n \rangle = 10^2$ to 10^6.

The discrete TLS formalism only approximates the effect of a sparse TLS spectral density where despite the spectral diffusion with a width Γ_2, and the random telegraph noise characterized by the rate γ, the coherent TLS spends most of its time detuned from the resonance. The assumptions of even energy spacing between TLS, $\Delta\epsilon$, and constant energy levels, are convenient for numerical evaluation of the model, but are not necessary to reproduce the loss reduction at low temperature. Two other estimations of the probability of the TLS being on resonance, as well as the number of strongly coupled fluctuators that can bring a detuned TLS into resonance, are given in Section S3, Supporting Information. Both calculations show that for any TLS with a spectral width Γ_2 and a detuning to the resonance ν, the TLS becomes less likely to be on resonance once $\Gamma_2(T) < \nu$ with decreasing temperature, qualitatively agreeing with the experimentally observed loss reduction at low temperature.

The treatment above is largely classical where the TLS are treated as dipoles under classical field. A quantum mechanical approach that studies the Jaynes–Cummings model of a single TLS strongly coupled to a photon predicts a linear temperature dependence of the loss similar to our observation.[84] However, it should be noted that the photon frequency in our measurement (3.64 GHz) corresponds to weak photon-TLS coupling, since the Rabi frequency from the effective field of a single photon is much weaker than the relaxation rates $\Gamma_{1,2}$. Additionally, the loss from strongly coupled TLS is predicted to show saturation in power at $\langle n \rangle \approx 1$, clearly lower than the observed saturation in the data at $\langle n \rangle \approx 10$ which corresponds to the weak coupling regime and reproduces the classical result.[84]

Although the fluctuators significantly affect the TLS internal loss, they should have limited effect on the frequency shifts.[72] The proposed discrete and detuned TLS formalism would not modify the STM frequency shift prediction either, because unlike the Lorentzian response function that governs the internal loss, the response function for frequency shift does not have a resonant shape and is not sensitive to the reduced sampling from the discrete TLS.

Ever since the importance of TLS interactions in amorphous solids was recognized by Yu and Leggett,[85] there have been numerous experimental works demonstrating evidence of TLS interactions,[70,76,86] and theoretical works treating the interacting TLS beyond STM,[87–89] with a recent example by Burin and Maksymov where they used a similar Master equation formalism.[28] However, the fluctuations in the energy levels are averaged over to form the spectral diffusion, unlike the fluctuators introduced by Faoro and Ioffe,[71,72] and the loss is predicted to have a power dependence faster than STM by a logarithmic factor, contrary to our observation.

At higher temperatures (above 150 mK), the quasiparticle effects become important, which corresponds to the upturn in loss in Figure 2. The quasiparticles loss is related to its density n_{qp} as

$$\frac{1}{Q_{\mathrm{qp}}} = \frac{2\alpha}{\pi}\frac{\sinh(\zeta)K_0(\zeta)n_{\mathrm{qp}}}{N_0\sqrt{2\pi k_{\mathrm{B}}T\Delta_{\mathrm{S0}}}}$$

$$\text{where} \quad n_{\mathrm{qp}} = n_{\mathrm{th}} + n_{\mathrm{noneq}} = 2N_0\sqrt{2\pi k_{\mathrm{B}}T\Delta_{\mathrm{S0}}} \times \exp\left(-\frac{\Delta_{\mathrm{S0}}}{k_{\mathrm{B}}T}\right) + n_{\mathrm{noneq}} \tag{15}$$

where n_{noneq} is the non-equilibrium quasiparticle density. Similar to the fit for frequency shift, the model with only n_{th} matches our data with the same set of fitting parameters $\Delta_0 = 170$ μeV and $\alpha = 0.014$. A calculation of the increased quasiparticle density including both thermal and non-equilibrium quasiparticles at high photon numbers in the half wavelength resonator based on Mattis–Bardeen equations[90,91] can be found in Section S5, Supporting Information. However, the results lack any strong temperature or power dependence below 100 mK. Note that this calculation includes the dynamics of the non-equilibrium quasiparticle finite lifetime due to recombination and trapping, with and without photon illumination.[92–95]

6. Conclusion

We have designed and fabricated capacitively-coupled half wavelength superconducting aluminum microwave resonators with minimum critical dimension of 1 μm in the center conducting line of the CPW. The temperature and power dependence of the resonator Q_i deviate from the classical standard tunneling model results. At high applied powers, the internal loss shows logarithmic power dependence, a signature of the generalized tunneling model with fluctuators. At powers below TLS saturation, the internal loss decreases from 50 mK down to the fridge base temperature. We attribute this behavior to the detuning between TLS and the resonance frequency in a discrete TLS ensemble. Upon cooling, the single TLS response bandwidth, proportional to $\Gamma_2 \propto T^{1.3}$, decreases. When the bandwidth drops below the detuning between TLS and the resonance frequency defined by the CPW resonator, the resonant TLS response decreases and contributes less to the internal loss. The generalized tunneling model is revisited and modified with the discrete TLS formalism resulting in a comprehensive fit to the measured loss in the entire low temperature and low power range, with a reasonable set of parameters.

Supporting Information

Supporting Information is available from the Wiley Online Library or from the author.

Acknowledgements

This work is funded by the US Department of Energy through Grant # DESC0018788 (sample preparation and measurements), and the National Science Foundation through Grant # NSF DMR-2004386. The authors acknowledge use of facilities at the Maryland Quantum Materials Center and the Maryland NanoCenter. The authors thank Rangga Budoyo and Braden Larsen for assistance with the non-equilibrium superconductor simulation. The authors thank Dr. Ben Palmer and Yizhou Huang at Laboratory for Physical Sciences for assistance with the thermal evaporator and helpful suggestions.

Conflict of Interest

The authors declare no conflict of interest.

Data Availability Statement

The data that support the findings of this study are available from the corresponding author upon reasonable request.

Keywords

dielectric loss, microwave superconductivity, superconducting resonators, two-level system

Received: October 19, 2022
Revised: October 27, 2023
Published online:

[1] J. Zmuidzinas, *Annu. Rev. Condens. Matter Phys.* **2012**, *3*, 169.
[2] J. J. A. Baselmans, S. J. C. Yates, *AIP Conf. Proc.* **2009**, *1185*, 160.
[3] P. Krantz, M. Kjaergaard, F. Yan, T. Orlando, S. Gustavsson, W. Oliver, *Appl. Phys. Rev.* **2019**, *6*, 021318.
[4] M. Kjaergaard, M. E. Schwartz, J. Braumüller, P. Krantz, J. I.-J. Wang, S. Gustavsson, W. D. Oliver, *Annu. Rev. Condens. Matter Phys.* **2020**, *11*, 369.
[5] M. D. Hutchings, J. B. Hertzberg, Y. Liu, N. T. Bronn, G. A. Keefe, M. Brink, J. M. Chow, B. L. T. Plourde, *Phys. Rev. Appl.* **2017**, *8*, 044003.
[6] J.-J. Chang, D. J. Scalapino, *Phys. Rev. B* **1977**, *15*, 2651.
[7] D. J. Goldie, S. Withington, *Supercond. Sci. Technol.* **2013**, *26*, 015004.
[8] P. J. de Visser, D. J. Goldie, P. Diener, S. Withington, J. J. A. Baselmans, T. M. Klapwijk, *Phys. Rev. Lett.* **2014**, *112*, 047004.

[9] R. P. Budoyo, Ph.D. Thesis, University of Maryland, College Park, MD **2015**.
[10] A. P. Vepsäläinen, A. H. Karamlou, J. L. Orrell, A. S. Dogra, B. Loer, F. Vasconcelos, D. K. Kim, A. J. Melville, B. M. Niedzielski, J. L. Yoder, S. Gustavsson, J. A. Formaggio, B. A. VanDevender, W. D. Oliver, *Nature* **2020**, *584*, 551.
[11] P. J. de Visser, J. J. A. Baselmans, P. Diener, S. J. C. Yates, A. Endo, T. M. Klapwijk, *Phys. Rev. Lett.* **2011**, *106*, 167004.
[12] R. Barends, J. Wenner, M. Lenander, Y. Chen, R. C. Bialczak, J. Kelly, E. Lucero, P. O'Malley, M. Mariantoni, D. Sank, H. Wang, T. C. White, Y. Yin, J. Zhao, A. N. Cleland, J. M. Martinis, J. J. A. Baselmans, *Appl. Phys. Lett.* **2011**, *99*, 113507.
[13] R. P. Budoyo, J. B. Hertzberg, C. J. Ballard, K. D. Voigt, J. R. A. Kim, C. J. Lobb, F. C. Wellstood, *Phys. Rev. B* **2016**, *93*, 024514.
[14] N. P. de Leon, K. M. Itoh, D. Kim, K. K. Mehta, T. E. Northup, H. Paik, B. S. Palmer, N. Samarth, S. Sangtawesin, D. W. Steuerman, *Science* **2021**, *372*, eabb2823.
[15] P. W. Anderson, B. I. Halperin, c. M. Varma, *Philos. Mag.: J. Theor. Exp. Appl. Phys.* **1972**, *25*, 1.
[16] W. A. Phillips, *J. Low Temp. Phys.* **1972**, *7*, 351.
[17] M. Von Schickfus, S. Hunklinger, *Phys. Lett. A* **1977**, *64*, 144.
[18] J. L. Black, B. I. Halperin, *Phys. Rev. B* **1977**, *16*, 2879.
[19] J. L. Black, *Phys. Rev. B* **1978**, *17*, 2740.
[20] W. A. Phillips, *Rep. Prog. Phys.* **1987**, *50*, 1657.
[21] J. M. Martinis, K. B. Cooper, R. McDermott, M. Steffen, M. Ansmann, K. D. Osborn, K. Cicak, S. Oh, D. P. Pappas, R. W. Simmonds, C. C. Yu, *Phys. Rev. Lett.* **2005**, *95*, 210503.
[22] J. Gao, J. Zmuidzinas, B. A. Mazin, H. G. LeDuc, P. K. Day, *Appl. Phys. Lett.* **2007**, *90*, 102507.
[23] J. Gao, M. Daal, A. Vayonakis, S. Kumar, J. Zmuidzinas, B. Sadoulet, B. A. Mazin, P. K. Day, H. G. Leduc, *Appl. Phys. Lett.* **2008**, *92*, 152505.
[24] A. D. O'Connell, M. Ansmann, R. C. Bialczak, M. Hofheinz, N. Katz, E. Lucero, C. McKenney, M. Neeley, H. Wang, E. M. Weig, A. N. Cleland, J. M. Martinis, *Appl. Phys. Lett.* **2008**, *92*, 112903.
[25] S. Kumar, J. Gao, J. Zmuidzinas, B. A. Mazin, H. G. LeDuc, P. K. Day, *Appl. Phys. Lett.* **2008**, *92*, 123503.
[26] R. Barends, H. L. Hortensius, T. Zijlstra, J. J. A. Baselmans, S. J. C. Yates, J. R. Gao, T. M. Klapwijk, *Appl. Phys. Lett.* **2008**, *92*, 223502.
[27] P. Macha, S. H. W. v. d. Ploeg, G. Oelsner, E. Il'ichev, H.-G. Meyer, S. Wünsch, M. Siegel, *Appl. Phys. Lett.* **2010**, *96*, 062503.
[28] A. L. Burin, A. O. Maksymov, *Phys. Rev. B* **2018**, *97*, 214208.
[29] C. Müller, J. H. Cole, J. Lisenfeld, *Rep. Prog. Phys.* **2019**, *82*, 124501.
[30] C. C. Yu, H. M. Carruzzo, in *Low-Temperature Thermal and Vibrational Properties of Disordered Solids* (Ed: M. A. Romas), World Scientific (Europe), London **2022**, pp. 113–139.
[31] A. M. Holder, K. D. Osborn, C. J. Lobb, C. B. Musgrave, *Phys. Rev. Lett.* **2013**, *111*, 065901.
[32] L. Gordon, H. Abu-Farsakh, A. Janotti, C. G. V. de Walle, *Sci. Rep.* **2014**, *4*, 7590.
[33] W. D. Oliver, P. B. Welander, *MRS Bull.* **2013**, *38*, 816.
[34] A. Bruno, G. de Lange, S. Asaad, K. L. van der Enden, N. K. Langford, L. DiCarlo, *Appl. Phys, Lett.* **2015**, *106*, 182601.
[35] G. Calusine, A. Melville, W. Woods, R. Das, C. Stull, V. Bolkhovsky, D. H. D. Braje, D. K. Kim, X. Miloshi, D. Rosenberg, A. Sevi, J. L. Yoder, E. Dauler, W. D. Oliver, *Appl. Phys. Lett.* **2018**, *112*, 1.
[36] A. Melville, G. Calusine, W. Woods, K. Serniak, E. Golden, B. M. Niedzielski, D. K. Kim, A. Sevi, J. L. Yoder, E. A. Dauler, W. D. Oliver, *Appl. Phys. Lett.* **2020**, *117*, 124004.
[37] J. M. Sage, V. Bolkhovsky, W. D. Oliver, B. Turek, P. B. Welander, *J. Appl. Phys.* **2011**, *109*, 063915.
[38] B. Chiaro, A. Megrant, A. Dunsworth, Z. Chen, R. Barends, B. Campbell, Y. Chen, A. Fowler, I. C. Hoi, E. Jeffrey, J. Kelly, J. Mutus, C. Neill, P. J. J. O'Malley, C. Quintana, P. Roushan, D. Sank, A. Vainsencher, J. Wenner, T. C. White1, J. M. Martinis, *Supercond. Sci. Technol.* **2016**, *29*, 104006.
[39] C. Richardson, A. Alexander, C. G. Weddle, B. Arey, M. Olszta, *J. Appl. Phys.* **2020**, *127*, 235302.
[40] A. Romanenko, R. Pilipenko, S. Zorzetti, D. Frolov, M. Awida, S. Belomestnykh, S. Posen, A. Grassellino, *Phys. Rev. Appl.* **2020**, *13*, 034032.
[41] S. E. de Graaf, L. Faoro, L. B. Ioffe, S. Mahashabde, J. J. Burnett, T. Lindström, S. E. Kubatkin, A. V. Danilov, A. Y. Tzalenchuk, *Sci. Adv.* **2020**, *6*, eabc5055.
[42] J. Jäckle, *Z. Phys. A: Hadrons Nuclei* **1972**, *257*, 212.
[43] S. Hunklinger, W. Arnold, in *Physical Acoustics* (Eds: W. P. Mason, R. N. Thurston), Vol. *12*, Academic Press, SanDiego, CA **1976**, pp. 155–215.
[44] C. Du, H. Chen, S. Li, *Phys. Rev. B* **2006**, *74*, 113105.
[45] A. L. Rakhmanov, A. M. Zagoskin, S. Savel'ev, F. Nori, *Phys. Rev. B* **2008**, *77*, 144507.
[46] P. Jung, A. V. Ustinov, S. M. Anlage, *Supercond. Sci. Technol.* **2014**, *27*, 073001.
[47] A. M. Zagoskin, D. Felbacq, E. Rousseau, *EPJ Quantum Technol.* **2016**, *3*, 2.
[48] N. Lazarides, G. P. Tsironis, *Phys. Rep.* **2018**, *752*, 1.
[49] J. Q. You, F. Nori, *Nature* **2011**, *474*, 589.
[50] P. Macha, G. Oelsner, J.-M. Reiner, M. Marthaler, S. André, G. Schön, U. Hübner, H.-G. Meyer, E. Il'ichev, A. V. Ustinov, *Nat. Commun.* **2014**, *5*, 5146.
[51] K. V. Shulga, E. Il'ichev, M. V. Fistul, I. S. Besedin, S. Butz, O. V. Astafiev, U. Hübner, A. V. Ustinov, *Nat. Commun.* **2018**, *9*, 150.
[52] Z. L. Xiang, S. Ashhab, J. Q. You, F. Nori, *Rev. Mod. Phys* **2013**, *85*, 623.
[53] S. I. Mukhin, M. V. Fistul, *Supercond. Sci. Technol.* **2013**, *26*, 084003.
[54] P. A. Volkov, M. V. Fistul, *Phys. Rev. B* **2014**, *89*, 054507.
[55] P. J. Petersan, S. M. Anlage, *J. Appl. Phys.* **1998**, *84*, 3392.
[56] S. J. Weber, K. W. Murch, D. H. Slichter, R. Vijay, I. Siddiqi, *Appl. Phys. Lett.* **2011**, *98*, 172510.
[57] J. Gao, Ph.D. Dissertation, Caltech, Department of Physics, Caltech, Pasadena, CA **2008**.
[58] C. R. H. McRae, H. Wang, J. Gao, M. R. Vissers, T. Brecht, A. Dunsworth, D. P. Pappas, J. Mutus, *Rev. Sci. Instrum.* **2020**, *91*, 091101.
[59] K. D. Crowley, R. A. McLellan, A. Dutta, N. Shumiya, A. P. Place, X. H. Le, Y. Gang, T. Madhavan, M. P. Bland, R. Chang, N. Khedkar, Y. C. Feng, E. A. Umbarkar, X. Gui, L. V. Rodgers, Y. Jia, M. M. Feldman, S. A. Lyon, M. Liu, R. J. Cava, A. A. Houck, N. P. de Leon, *Phys. Rev. X* **2023**, *13*, 041005.
[60] J. Burnett, L. Faoro, T. Lindstrom, *Supercond. Sci. Technol.* **2016**, *29*, 044008.
[61] J. Gao, J. Zmuidzinas, A. Vayonakis, P. Day, B. Mazin, H. Leduc, *J. Low Temp. Phys.* **2008**, *151*, 557.
[62] D. P. Pappas, M. R. Vissers, D. S. Wisbey, J. S. Kline, J. Gao, *IEEE Trans. Appl. Supercond.* **2011**, *21*, 871.
[63] H. Wang, M. Hofheinz, J. Wenner, M. Ansmann, R. C. Bialczak, M. Lenander, E. Lucero, M. Neeley, A. D. O'Connell, D. Sank, M. Weides, A. N. Cleland, J. M. Martinis, *Appl. Phys. Lett.* **2009**, *95*, 233508.
[64] M. S. Khalil, F. C. Wellstood, K. D. Osborn, *IEEE Trans. Appl. Supercond.* **2011**, *21*, 879.
[65] M. Schechter, P. C. E. Stamp, *J. Phys.: Condens. Matter* **2008**, *20*, 244136.
[66] M. S. Khalil, M. J. A. Stoutimore, S. Gladchenko, A. M. Holder, C. B. Musgrave, A. C. Kozen, G. Rubloff, Y. Q. Liu, R. G. Gordon, J. H. Yum, S. K. Banerjee, C. J. Lobb, K. D. Osborn, *Appl. Phys. Lett.* **2013**, *103*, 162601.
[67] M. Schechter, P. C. E. Stamp, *Phys. Rev. B* **2013**, *88*, 174202.

[68] M. Schechter, P. Nalbach, A. L. Burin, *New J. Phys.* **2018**, *20*, 063048.
[69] L. Yu, S. Matityahu, Y. J. Rosen, C.-C. Hung, A. Maksymov, A. L. Burin, M. Schechter, K. D. Osborn, *Sci. Rep.* **2022**, *12*, 16960.
[70] J. Burnett, L. Faoro, I. Wisby, V. L. Gurtovoi, A. V. Chernykh, G. M. Mikhailov, V. A. Tulin, R. Shaikhaidarov, V. Antonov, P. J. Meeson, A. Y. Tzalenchuk, T. Lindström, *Nat. Commun.* **2014**, *5*, 4119.
[71] L. Faoro, L. B. Ioffe, *Phys. Rev. Lett.* **2012**, *109*, 157005.
[72] L. Faoro, L. B. Ioffe, *Phys. Rev. B* **2015**, *91*, 014201.
[73] E. Cuevas, R. Chicón, M. Ortuño, *Phys. B* **1989**, *160*, 293.
[74] A. Churkin, S. Matityahu, A. O. Maksymov, A. L. Burin, M. Schechter, *Phys. Rev. B* **2021**, *103*, 054202.
[75] R. Jankowiak, G. J. Small, *Chem. Phys. Lett.* **1993**, *207*, 436.
[76] J. Gao, M. Daal, J. M. Martinis, A. Vayonakis, J. Zmuidzinas, B. Sadoulet, B. A. Mazin, P. K. Day, H. G. Leduc, *Appl. Phys. Lett.* **2008**, *92*, 212504.
[77] S. Kumar, J. Gao, J. Zmuidzinas, B. A. Mazin, H. G. LeDuc, P. K. Day, *Appl. Phys. Lett.* **2008**, *92*, 123503.
[78] S. E. de Graaf, S. Mahashabde, S. E. Kubatkin, A. Y. Tzalenchuk, A. V. Danilov, *Phys. Rev. B* **2021**, *103*, 174103.
[79] B. Sarabi, Ph.D. Thesis, University of Maryland, College Park, MA **2014**.
[80] J. Lisenfeld, C. Müller, J. H. Cole, P. Bushev, A. Lukashenko, A. Shnirman, A. V. Ustinov, *Phys. Rev. Lett.* **2010**, *105*, 230504.
[81] G. J. Grabovskij, T. Peichl, J. Lisenfeld, G. Weiss, A. V. Ustinov, *Science* **2012**, *338*, 232.
[82] B. Sarabi, A. N. Ramanayaka, A. L. Burin, F. C. Wellstood, K. D. Osborn, *Phys. Rev. Lett.* **2016**, *116*, 167002.
[83] C.-C. Hung, L. Yu, N. Foroozani, S. Fritz, D. Gerthsen, K. D. Osborn, *Phys. Rev. Appl.* **2022**, *17*, 034025.
[84] M. Bhattacharya, K. D. Osborn, A. Mizel, *Phys. Rev. B* **2011**, *84*, 104517.
[85] C. Yu, A. Leggett, *Comments Cond. Mat. Phys* **1988**, *14*, 231.
[86] J. Lisenfeld, G. J. Grabovskij, C. Müller, J. H. Cole, G. Weiss, A. V. Ustinov, *Nat. Commun.* **2015**, *6*, 6182.
[87] S. N. Coppersmith, *Phys. Rev. Lett.* **1991**, *67*, 2315.
[88] A. L. Burin, Y. Kagan, *Phys. B* **1994**, *194–196*, 393.
[89] D. C. Vural, A. J. Leggett, *J. Non-Cryst. Solids* **2011**, *357*, 3528.
[90] D. C. Mattis, J. Bardeen, *Phys. Rev.* **1958**, *111*, 412.
[91] J. P. Turneaure, J. Halbritter, H. A. Schwettman, *J. Supercond.* **1991**, *4*, 341.
[92] A. Rothwarf, B. N. Taylor, *Phys. Rev. Lett.* **1967**, *19*, 27.
[93] W. H. Parker, *Phys. Rev. B* **1975**, *12*, 3667.
[94] T. Guruswamy, D. J. Goldie, S. Withington, *Supercond. Sci. Technol.* **2015**, *28*, 054002.
[95] L. Grünhaupt, N. Maleeva, S. T. Skacel, M. Calvo, F. Levy-Bertrand, A. V. Ustinov, H. Rotzinger, A. Monfardini, G. Catelani, I. M. Pop, *Phys. Rev. Lett.* **2018**, *121*, 117001.